Length-Dependent Thermal Transport along Molecular Chains

T. Meier,[1,2] F. Menges,[1,3] P. Nirmalraj,[1] H. Hölscher,[2] H. Riel,[1] and B. Gotsmann[1]
[1]IBM Research-Zurich, Säumerstrasse 4, CH-8803 Rüschlikon, Switzerland
[2]Institute of Microstructure Technology, Karlsruhe Institute of Technology (KIT), Hermann-von-Helmholtz Platz 1, D-76344 Eggenstein-Leopoldshafen, Germany
[3]Nanotechnology Group, ETH Zürich, Säumerstrasse 4, CH-8803 Rüschlikon, Switzerland
(Received 14 April 2014; published 8 August 2014)

We present heat-transport measurements conducted with a vacuum-operated scanning thermal microscope to study the thermal conductance of monolayers of nine different alkane thiols self-assembled on Au(111) surfaces as a function of their length (2 to 18 methylene units). The molecular thermal conductance is probed in a confined area with a diameter below 10 nm in the contact between a silicon tip and the self-assembled monolayer. This yields a pWK^{-1} sensitivity per molecule at a tip temperature of 200–300 °C versus the gold at room temperature. We found a conductance variance of up to a factor of 3 as a function of alkane chain length, with maximum conductance for a chain length of four carbon atoms.

DOI: 10.1103/PhysRevLett.113.060801 PACS numbers: 68.90.+g, 07.79.-v, 68.55.am

One-dimensional chains of springs and masses are peculiar systems. Although they are many-particle systems, they do not behave like thermodynamic ensembles as they do not equilibrate [1]. This leads to untypical behavior in terms of thermal transport also. Specifically, 1D chains do not follow Fourier's law [2,3]

$$\dot{Q} = k\nabla T,$$

equating the heat flux $\dot{Q}$ to the constant thermal conductivity k times the temperature gradient ∇T. However, for linear (1D) chains, it is found that the thermal conductivity diverges with chain length $k \propto N^{\alpha}$, with $\alpha > 0$, instead of being a material-intrinsic property as required for Fourier's law ($k = \text{const}$ or $\alpha = 0$). After extensive investigation [2–4], it was concluded from simulations that $\alpha = 1/3$ is a typical value for long chains ($N > 100$). The thermal conductance of a single chain, $G_m = \dot{Q}/\Delta T$, (units W/K), scales with the thermal conductivity k like $G_m \propto k/L$, where L is the length of the chain increasing in proportion to N, and therefore, $G_m \propto N^{\alpha-1}$.

Extending this insight to shorter chains is of high technological relevance [5]. For example, self-assembled monolayers (SAMs) of alkane chains on surfaces [6] are candidates for electronic and sensor applications and energy conversion, where thermal transport is of relevance.

Simulations of short chains ($N < 100$) indicated that the coupling strength between the chains and the thermal reservoirs governs [2,7–9] α values ranging from 0 to 1. Indeed, a strong dependence of the conductance on the coupling of molecular chains (SAMs) to one [10,11] or two thermal reservoirs [12–14] has been demonstrated experimentally. However, the length dependence of 1D (or molecular) conductance for short chains is yet to be fully understood. Molecular dynamics simulations of SAMs [9] predict significant phonon interference effects with conductance variations of about a factor of 3 as a function of N, for $N = 3$, 8, 16, and 32. In a more detailed quantum-mechanical simulation of single molecules, Segal *et al.* [7] also predict conductance variations, but with a single maximum at $N = 4$ and approaching a constant conductance for $N > 20$ for the weakly coupled case and $\alpha \approx 0$ for the strongly coupled case. In contrast, Duda *et al.* [15] argue that the thermal conductance is ballistic and independent of length ($\alpha = 0$) for $N \geq 5$ because of a length-independent density of phonon states.

Experimental data of SAMs sandwiched between gold and gallium arsenide surfaces [12] or between gold and water [10] is too scarce to allow the extraction of a length dependence. Time-resolved flash heating experiments of SAMs through the gold substrate [11] ($N = 6$ to 24) were fitted to a length dependence of the equilibration time to $\tau \propto (N - N_0)$, with an offset $N_0 \approx 3$. The offset implies a diverging conductance for N approaching N_0 and, therefore, a deviation from a simple proportionality ($k \propto N$) corresponding to constant conductance. However, the opposite trend was obtained [16] when measuring and simulating intramolecular equilibration times through alkane linkers, namely, a Fourier-like trend ($\alpha = 0$) for $N \leq 4$ and constant conductance ($\alpha = 1$) for $N = 5$ to 8.

In this Letter, we measured the length dependence of thermal transport across alkane SAMs using scanning thermal microscopy (SThM) [17]. Here, the alkane molecules are sandwiched between a gold-thiol bond (strong coupling) and the silicon SThM tip (weak coupling), see Fig. 1(a). SThM offers the advantage of a local imaging method for simultaneously mapping and correlating the samples' topography and heat flux to identify local defects, such as grain boundaries, and point defects of the gold substrate and film [17]. In electrical transport measurements,

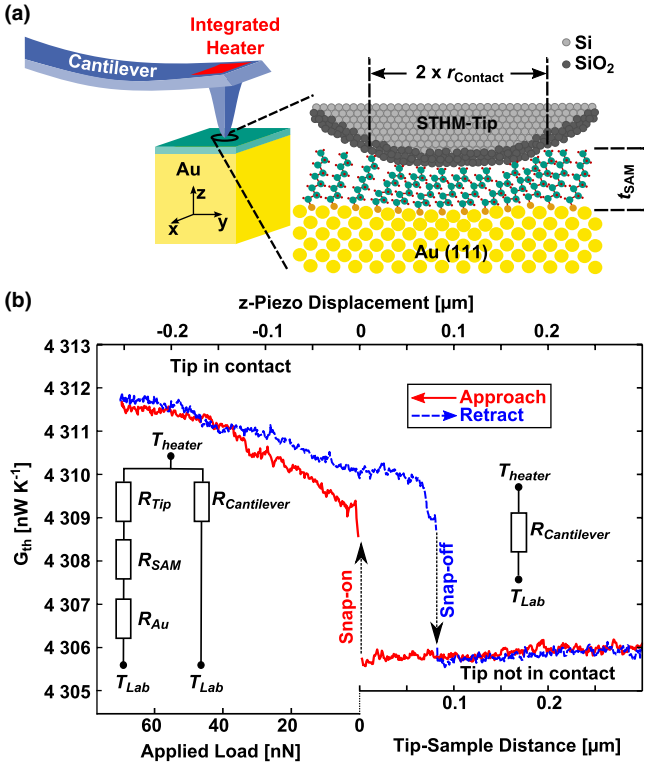

FIG. 1 (color online). (a) Schematic of the contact geometry. The contact radius, r_{Contact}, is a function of the applied load and the thickness of the SAM, t_{SAM}. (b) Example of thermal conductance versus displacement measurement on octadecanethiol. During contacting the sample with the tip, the heat flow from the heated tip through cantilever and sample is recorded. By analyzing the noncontact and the contact regime of the thermal conductance versus displacement curves and the geometry of the tip-sample contact, the thermal conductance of the SAM can be extracted in a space-resolved manner. The applied z-piezo displacement (top axis) translates into a variation of the tip-sample distance or the load force when the tip is not in contact or in contact with the surface (bottom axes), respectively.

such defects have been identified as a major cause of nonreproducibility [18]. By using repeated contacting-detaching cycles of the tip and the surface rather than scanning images, as described below, we avoid wear, achieve excellent reproducibility, and obtain sufficient sensitivity.

We used samples of highly ordered SAMs of alkane thiols $[\mathrm{HS}\text{-}(\mathrm{CH}_2)_{N-1}\text{-}\mathrm{CH}_3]$, with $N = 2, 3, 4, 8, 12, 14, 16$, and 18 methylene units, on Au(111) substrates on Mica. Samples were prepared following the procedure described by Delamarche *et al.* [19] to obtain uniform monolayers. The SAM film preparation procedure was confirmed using the usual thin film characterization methods such as ellipsometry and scanning probe microscopy (intermittent-contact mode atomic force microscopy). Using a custom-built SThM [20] operated under vacuum in a noise-free lab [21] with home-built silicon sensors or tips [22], we introduce a thermal force mapping technique. The silicon sensor, which was calibrated using a procedure described by Menges *et al.* [20], detects the temperature-dependent resistance of a low-doped silicon region.

On each sample, we performed the thermal force mapping by repeatedly obtaining thermal contact curves as shown in Fig. 1(b) and recording the thermal conductance, G_{th}, versus the displacement of the piezo element carrying the cantilevered heater sensor with the tip. The cantilever's thermal resistance is extracted from the measured response on the heater sensor without tip-surface contact. With the tip in contact, an increase of conductance is measured which is assigned to the tip-surface heat path. With a stepwise lateral movement of the sample under the tip between individual thermal conductance-versus-displacement curves, a high spatial resolution is obtained.

For high load forces, a threshold pressure is reached and the tip starts to punch through the SAM and touches the gold substrate directly [23]. To limit the pressure, we used a relatively blunt tip with a radius of 28 nm allowing us to apply several tens of nN before a punch through [24].

The thermal conductance measured [Fig. 2(a)] varies with the piezo position as the resulting contact force enhances the tip load on the surface and subsequently increases the contact area. To obtain the thermal conductance per unit area G_A and, hence, the conductance per molecule G_m, the tip-SAM contact area has to be determined and combined with the SAM density of 0.214 nm^2 per molecule [18]. A universal contact model for the layered system SAM (of thickness t_{SAM}) on gold is not available. However, for sufficiently large contact radii, where the contact radius is larger than the film thickness ($r_{\mathrm{contact}} > t_{\mathrm{SAM}}$), a thin-film compression model applies to this system [44,45] and was used to calculate the contact area versus load [see Fig. 2(b)] and [24]]. One of the largest sources of error in the data analysis is the uncertainty of the tip-surface adhesion force. Within the limits of the statistical scattering of the measured adhesion force, we treat the adhesion force as a fit parameter to optimize for a constant thermal conductance per unit area for any given SAM [24]. As depicted in Fig. 2(c), curves of constant G_A are obtained, except at low loads, where the model assumptions do not apply. Because of the large thermal conductivity of gold and silicon, the spreading resistances in tip and substrate contribute only a negligible offset [24].

Compared with conventional surface scans, approach and retraction of the tip to and from the sample greatly simplify the contact mechanics because of the absence of friction forces. Furthermore, avoiding shear forces occurring during sliding motion helps minimize wear and contamination and, thereby, preserves the integrity of tip and surface for subsequent measurements. Measuring contact curves on 60×60 locations of the surface of each sample separated by 16 nm results in maps of the topography, the adhesion force, and the load force dependence of the thermal conductance of the sample with high

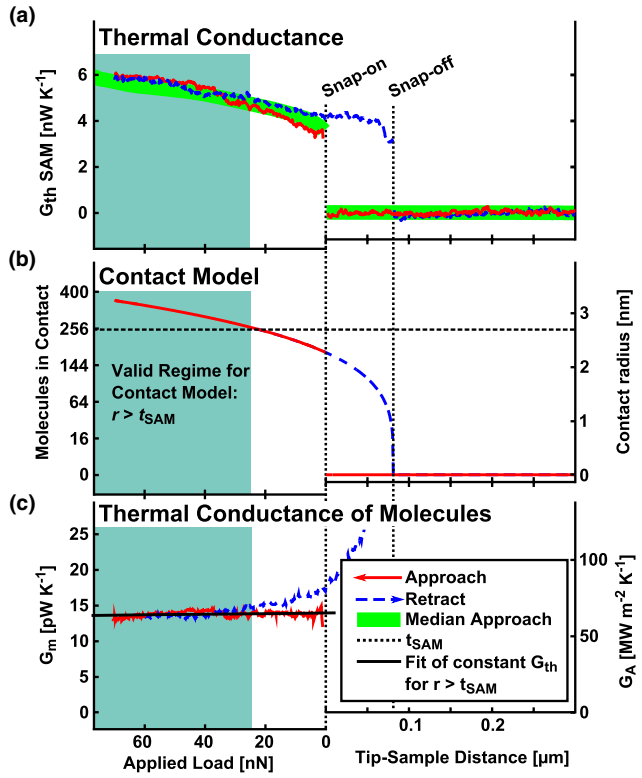

FIG. 2 (color online). Example of analysis of the molecular thermal conductance using a contacting curve of an octadecanethiol SAM. (a) Results of translating the contacting curve of Fig. 1(b) into conductance versus applied load. Also shown is the average over 2500 such curves. The contact model applicable to this sample is plotted in (b); the shaded region denotes the region of validity of the model. Combining the data of (a) and (b), the thermal conductance per unit area, G_A, or per molecule, G_m, can be extracted, as shown in (c). Taking the measured distance between snap-on and snap-off points multiplied by the spring constant of the cantilever as the adhesion force, F_{adh}, an almost constant G_A or G_m is obtained. In the batch analysis, F_{adh} is treated as a fit parameter to increase accuracy.

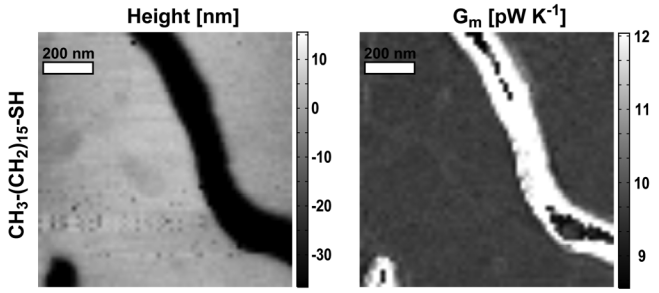

FIG. 3. Example of topography (left) and thermal conductance (right) maps. The high spatial resolution of scanning-probe-based thermal mapping allows the identification of topographic artifacts and structural defects in the thermal conductance measured that cause nonreproducibility. A gap between two gold islands, for example, appears dark in the topography and white in the thermal conductance map. We excluded such defects on the samples from further analysis.

spatial resolution, as shown in Fig. 3. This allows us to identify and discard data taken in regions with step edges and defects of the sample surface. To obtain the thermal conductance per molecule, measurements with tip temperatures of 200 °C and 300 °C and peak forces keeping the integrity of the tip and SAM intact were recorded on multiple positions on the samples [24]. We used the approach curve of the data which is less affected by the typical systematic errors of scanning probe-based contacting curves. After discarding the results for areas with defects on the samples, the remaining thermal contact curves were analyzed and averaged for each chain length

Figure 4 shows the thermal conductance as a function of the chain length N. Short-chain samples ($N \leq 4$) are significantly more conductive than the longer-chain samples with a maximum conductance at $N = 4$. An overall decaying trend of conductance versus chain length is observed. Despite the scatter in the data, some significant conclusions can be drawn through comparison of existing models and simulations. The following comparison assumes that models and simulations can be applied even though the temperature bias is rather large in this particular experiment. The present data do not allow us to make solid conclusions on the temperature dependence. Furthermore, 1D transport is assumed [24].

An overall decaying trend can be fitted empirically with $G = \dot{Q}/\Delta T \propto k/t_{SAM} \propto N^{\alpha-1}$, resulting in an exponent $\alpha = 0.64 \pm 0.2$ (from least squares). Since it has been argued that, for very short chains, different effects may play a role (see below), it is interesting to make a similar fit only for the longer chains ($N = 4$ to 18) from which we find $\alpha = 0.38 \pm 0.2$. In either case, the exponent is not compatible with either constant ($\alpha = 1$, as in ballistic transport) or Fourier-like ($\alpha = 0$, as in diffusive transport) conductance. At first sight, this may be indicative of a situation in which transport is neither purely ballistic nor diffusive, i.e., quasiballistic transport with a phonon mean free path Λ on the same order as the chain length [46], following $G \propto (N + \Lambda)^{-1}$. (Here, the mean free path Λ is expressed in multiples of CH_2 units of the molecular backbone.) This results in a decaying conductance with length, and a fit to our data yields $\Lambda \approx 5$; however, such a short mean free path is in striking contrast to the mean free path of 40 nm we estimated from the thermal conductance measured using crystals of alkane chains (polyethylene) [47].

One alternative concept, describing ballistic transport and potentially leading to an increased heat transfer for shorter chains, is based on the assumption that the mechanical coupling between the two contacts works directly: Rather than viewing the ballistic transport as a series of steps, transmitting phonons into the molecule, propagation through the molecule, and transmitting out of the molecule, in this view, the molecule serves as a link to directly couple both contacts. For example, using a continuum-mechanics

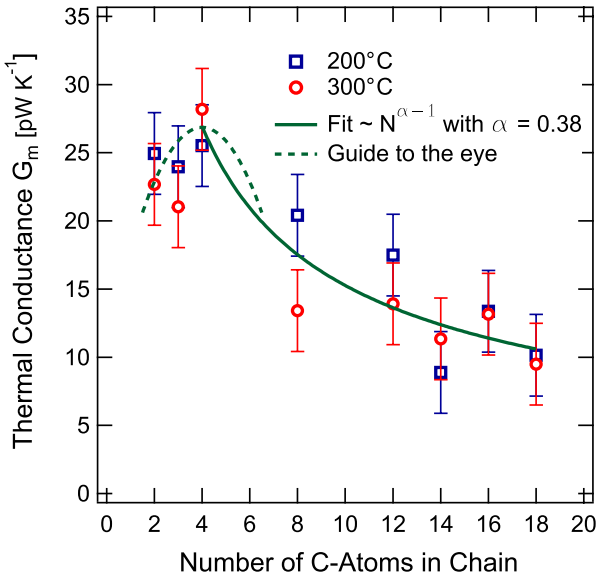

FIG. 4 (color online). Molecular thermal conductance as a function of chain length for two heater temperatures. The thermal conductance can be fitted with an $\alpha = 0.38 \pm 0.2$ for chain lengths longer than four carbon atoms in the chain. For shorter chains, the reduction of vibrational modes in the chain decreases the thermal conductance again, revealing a peak conductance around four carbon atoms per chain within the limits and errors of the experiment. While experimental scatter is given in the error bars, a systematic error offsetting all data by ±42% is excluded (see Supplemental Material [24]).

model, we neglect the internal vibration modes of the molecules and model the coupling between the silicon tip and gold through the SAM with single springs using the SAM's Young's modulus (40 ± 20 GPa) [48]. With a suitable offset of 8 pWK^{-1} accounting for ballistic low-frequency phonons, this allows us to quantitatively describe the data for $N = 4$ to 18. Still, the model predicts an even better mechanical coupling for $N = 2$ or 3, with at least 1 order of magnitude enhanced conductance between $N = 2$ and $N = 4$, in contrast to our observation even when taking into account the uncertainty of the experiment. Therefore, it appears likely that the internal vibrational properties of the SAM layer play an increasing role in the increased phonon transmission for a decreasing chain length in the temperature range applied here.

A more plausible scenario is to stay with the assumption of ballistic transport through the carbon chains [2,3,7,15], i.e., assuming a mean free path Λ greater than the chain lengths studied here and using a Landauer model of transport. In this picture, a variation in conductance is related either to a variation of the density of phonon modes in the molecule or a variation in transmission probability through existing modes. The first option has already been addressed by calculating the phonon spectra of molecular junctions [7,15]. It was found that the number of vibronic states increases in proportion to N, with an approximately constant density of states. From this, it can be argued that the conductance should be constant and an interface-governed ballistic thermal transport effect [11,13,15]. Within its uncertainty, the data are consistent with this prediction of constant conductance for $N \geq 14$.

The conductance enhancement for shorter chains requires a variation of transmission probability through existing phonon frequency modes as a function of chain length. This may originate from phonon interference effects within the alkane chains. Simulation data [9], however, is available only for a few chain lengths, and therefore, a trend cannot easily be extracted. The phonon-frequency-dependent transmission was also calculated by Segal *et al.* [7] using quantum mechanics. They observe a contribution to heat conduction by higher-frequency phonons within the molecule coupled to the low-frequency phonons responsible for heat transport in the reservoirs. They expect this coupling to weaken exponentially with N and, thereby, to reduce the overall conductance. The reasons for this effect are not yet understood, but a correlation with frequency-dependent phonon localization effects [3,7] has been pointed out [11].

The calculations by Segal *et al.* [7] also predict an increase of conductance for chains with $N < 20$ very similar to our observation. Furthermore, a stagnation of conductance for short chains and a maximum conductance at $N = 4$ is predicted. This stagnation is consistent with our data (see guide to the eye in Fig. 4), although the error bars of the data are too large to allow a solid conclusion on the trend for $N \leq 4$. Nevertheless, the behavior predicted by Segal *et al.* [7] matches our data well.

In conclusion, we achieved sufficient sensitivity to quantify the thermal conductance of alkane-thiol SAMs as a function of chain length by applying a thermal force mapping technique to scanning thermal microscopy. We resolved variations in the chain-length-dependent thermal conductance of a factor of 3, with a maximal conductance for four methylene units per chain. The decaying trend for $N \geq 4$ neither satisfies requirements of diffusive transport nor exhibits constant conductance as previously predicted. For longer alkane chains, we found a diverging conductance, similar to what is expected for very long chains.

It is a pleasure to thank Heiko Wolf, Walter Riess and Emanuel Lörtscher for fruitful discussions and technical assistance. The research leading to these results has received funding from the Karlsruhe House of Young Scientists, the European Union Seventh Framework Programs (No. FP7/2007-2013) Nanoheat under Grant agreement No. (318625), and the Swiss Science Foundation Project No. 134777.

[1] E. Fermi, J. Pasta, and S. Ulam, Los Alamos Report No. LA-1940, 1955.
[2] S. Lepri, R. Livi, and A. Politi, Phys. Rep. **377**, 1 (2003).
[3] A. Dhar, Adv. Phys. **57**, 457 (2008).

[4] R. Peierls, Ann. Phys. (Berlin) **395**, 1055 (1929).
[5] D. Witt, R. Klajn, P. Barski, and B. A. Grzybowski, Curr. Org. Chem. **8**, 1763 (2004).
[6] A. Ulman, Chem. Rev. **96**, 1533 (1996).
[7] D. Segal, A. Nitzan, and P. Hänggi, J. Chem. Phys. **119**, 6840 (2003).
[8] M. A. Panzer and K. E. Goodson, J. Appl. Phys. **103**, 094301 (2008).
[9] L. Hu, L. Zhang, M. Hu, J.-S. Wang, B. Li, and P. Keblinski, Phys. Rev. B **81**, 235427 (2010).
[10] Z. Ge, D. G. Cahill, and P. V. Braun, Phys. Rev. Lett. **96**, 186101 (2006).
[11] Z. Wang, J. A. Carter, A. Lagutchev, Y. K. Koh, N.-H. Seong, D. G. Cahill, and D. D. Dlott, Science **317**, 787 (2007).
[12] R. Y. Wang, R. A. Segalman, and A. Majumdar, Appl. Phys. Lett. **89**, 173113 (2006).
[13] M. D. Losego, M. E. Grady, N. R. Sottos, D. G. Cahill, and P. V. Braun, Nat. Mater. **11**, 502 (2012).
[14] P. J. O' Brien, S. Shenogin, J. Liu, P. K. Chow, D. Laurencin, P. H. Mutin, M. Yamaguchi, P. Keblinski, and G. Ramanath, Nat. Mater. **12**, 118 (2013).
[15] J. C. Duda, C. B. Saltonstall, P. M. Norris, and P. E. Hopkins, J. Chem. Phys. **134**, 094704 (2011).
[16] D. Schwarzer, P. Kutne, C. Schröder, and J. Troe, J. Chem. Phys. **121**, 1754 (2004).
[17] A. Majumdar, Annu. Rev. Mater. Sci. **29**, 505 (1999).
[18] J. C. Love, L. A. Estroff, J. K. Kriebel, R. G. Nuzzo, and G. M. Whitesides, Chem. Rev. **105**, 1103 (2005).
[19] E. Delamarche, B. Michel, C. Gerber, D. Anselmetti, H.-J. Guentherodt, H. Wolf, and H. Ringsdorf, Langmuir **10**, 2869 (1994).
[20] F. Menges, H. Riel, A. Stemmer, and B. Gotsmann, Nano Lett. **12**, 596 (2012).
[21] E. Lortscher, D. Widmer, and B. Gotsmann, Nanoscale **5**, 10542 (2013).
[22] U. Drechsler, N. Bürer, M. Despont, U. Dürig, B. Gotsmann, F. Robin, and P. Vettiger, Microelectron. Eng. **67–68**, 397 (2003).
[23] R. W. Carpick and M. Salmeron, Chem. Rev. **97**, 1163 (1997).
[24] See Supplemental Material at http://link.aps.org/supplemental/10.1103/PhysRevLett.113.060801 for details on the setup, the temperature calibration, the contact mechanics and the one-dimensional character of SAMS, which includes Refs. [25–43].
[25] M. Hinz, O. Marti, B. Gotsmann, M. A. Lantz, and U. Dürig, Appl. Phys. Lett. **92**, 043122 (2008).
[26] B. Gotsmann, M. Lanz, A. Knoll, and U. Dürig, in *Nanotechnology*, Vol. 2 (Verlag GmbH & Co. KGaA, New York, 2010), p. 043122.
[27] D. Wiesmann and A. Sebastian, in *19th IEEE International Conference on Micro Electro Mechanical Systems, 2006. MEMS 2006 Istanbul.* (IEEE, New York, 2006), pp. 182–185.
[28] K. J. Kim and W. P. King, Applied Thermal Engineering **29**, 1631 (2009).
[29] S. M. Sze and K. K. Ng, *Physics of Semiconductor Devices*, 3rd ed. (Wiley, New York, 2007).
[30] K. L. Johnson, *Contact Mechanics*, 9th ed. (Cambridge University Press, Cambridge, England, 2003).
[31] S. J. Cole and R. S. Sayles, J. Tribol. **114**, 334 (1992).
[32] B. N. J. Persson, A. I. Volokitin, and H. Ueba, J. Phys. Condens. Matter **23**, 045009 (2011).
[33] R. Prasher, Appl. Phys. Lett. **94**, 041905 (2009).
[34] B. Derjaguin, V. Muller, and Y. Toporov, J. Colloid Interface Sci. **53**, 314 (1975).
[35] K. M. Balss, G. A. Fried, and P. W. Bohn, J. Electrochem. Soc. **149**, C450 (2002).
[36] M. A. Poggi, L. A. Bottomley, and P. T. Lillehei, Nano Lett. **4**, 61 (2004).
[37] L. Ramin and A. Jabbarzadeh, Model. Simul. Mater. Sci. Eng. **20**, 085010 (2012).
[38] L. Costelle, P. Jalkanen, M. T. Risnen, L. Lind, R. Nowak, and J. Risnen, J. Appl. Phys. **110**, 114301 (2011).
[39] K. Kurabayashi, Int. J. Thermophys. **22**, 277 (2001).
[40] K. Kurabayashi, M. Asheghi, M. Touzelbaev, and K. E. Goodson, J. Microelectromech. Syst. **8**, 180 (1999).
[41] G. Chen, *Nanoscale Energy Transport and Conversion: a Parallel Treatment of Electrons, Molecules, Phonons, and Photons*, MIT-Pappalardo Series in Mechanical Engineering (Oxford University Press, Oxford, 2005).
[42] G. Dames and G. Chen, *Thermoelectrics Handbook: Macro to Nano* (CRC Press, Boca Raton, FL, 2006), Chap. 42.
[43] D. Li, Y. Wu, P. Kim, L. Shi, P. Yang, and A. Majumdar, Appl. Phys. Lett. **83**, 2934 (2003).
[44] B. Bhushan and W. Peng, Appl. Mech. Rev. **55**, 435 (2002).
[45] E. Gacoin, C. Fretigny, A. Chateauminois, A. Perriot, and E. Barthel, Tribol. Lett. **21**, 245 (2006).
[46] D. Roy, Phys. Rev. E **77**, 062102 (2008).
[47] S. Shen, A. Henry, J. Tong, R. Zheng, and G. Chen, Nat. Nanotechnol. **5**, 251 (2010).
[48] K. R. Patton and M. R. Geller, Phys. Rev. B **64**, 155320 (2001).